Available online at www.sciencedirect.com

SciVerse ScienceDirect

Ceramics International 38 (2012) 3901–3906

CERAMICS INTERNATIONAL

www.elsevier.com/locate/ceramint

Photocatalytic characteristics of immobilized $SrBi_2Nb_2O_9$ film for degradation of organic pollutants

Jin-Ho Kim [a,*], Kwang-Taek Hwang [a], Ung-Soo Kim [a], Yong-Mook Kang [b]

[a] *Icheon Branch, Korea Institute of Ceramic Engineering & Technology (KICET), Icheon-si, Gyeonggi-do, Republic of Korea*

[b] *Division of Advanced Materials Engineering, Kongju National University, 275, Budae-dong, Cheonan, Chungnam 330-717, Republic of Korea*

Received 5 December 2011; received in revised form 16 January 2012; accepted 16 January 2012

Available online 4 February 2012

Abstract

The use of semiconducting oxide photocatalyst in contaminant purification has recently drawn significant attention in both materials and environmental science. In this study, the compound $SrBi_2Nb_2O_9$ with layered perovskite-type structure was synthesized by solid state reaction, and the network microstructure film was fabricated by the aerosol deposition method. The compound powder and aerosol-deposited film with $SrBi_2Nb_2O_9$ were characterized by X-ray diffraction (XRD), scanning electron microscopy (SEM) and Ultra violet–visible (UV–vis) spectrophotometry. The photocatalytic activity of the aerosol-deposited film with $SrBi_2Nb_2O_9$ was evaluated by photo-induced destruction of Rhodamine B under the irradiation of UV and visible light. The aerosol-deposited film with $SrBi_2Nb_2O_9$ exhibited higher photocatalytic activity than that of $SrBi_2Nb_2O_9$ powders. This result is attributed not only to the small sized grain, but also to the existence of a network microstructure capable of supporting the enhanced loading of organic contaminants on the aerosol-deposited film.

Keywords: Semiconducting oxide photocatalyst; $SrBi_2Nb_2O_9$; Aerosol deposition; Photocatalytic activity; Rhodamine B

1. Introduction

In recent years, semiconducting oxide photocatalysts have attracted extensive attention because of their potential applications in solar energy conversion and environmental purification [1–4]. There has been a significant amount of research on the decomposition of environmental pollutants and the destruction of bacteria using photocatalytic TiO_2 ever since Fujishima and Handa reported water splitting using a TiO_2 photoelectrode [1]. TiO_2 has been known for its good environmental stability and excellent photocatalytic activity [5,6]. However, the practical applications of photocatalytic TiO_2 have been hindered primarily by its low quantum yield and lack of visible-light utilization. Therefore, many researchers have focused their efforts on the design and development of single phase oxide photocatalysts working under visible light illumination [7–10].

Compounds of the general formula $A_{m-1}Bi_2M_mO_{3m+3}$ ($m = 1$, 2, 3, and 4) were first synthesized by Aurivillius [11]. The crystal structure of Aurivillius-type oxides can be regarded as a regular intergrowth of $(Bi_2O_2)^{2+}$ fluorite layers and $(A_{m-1}M_mO_{3m+1})^{2-}$ pseudo-perovskite slabs. The structure allows a wide variety of chemical substitution at the A and M sites, thereby exhibiting an enormous range of physical properties. Recently, Li et al. reported the photocatalytic activities of Aurivillius-type $ABi_2Nb_2O_9$ (A = Sr, Ca, Ba) powders on water splitting under UV-light irradiation. In their investigation, $SrBi_2Nb_2O_9$ showed the highest evolution rate of H_2 and O_2 [12]. Also, Wu et al. studied the photocatalytic activity of microcrystalline $ABi_2Nb_2O_9$ (A = Sr, Ba) compounds synthesized by a citrate complex method [13]. They reported that $SrBi_2Nb_2O_9$ exhibited higher photocatalytic activity than that of $BaBi_2Nb_2O_9$ for the photocatalytic redox reaction of methyl orange under UV light irradiation.

In general, most of the studies on photocatalytic activities have focused on the powder form of photocatalysts. However, there are two practical problems with using powders in photocatalytic processing: (1) it is difficult to separate the catalysts from the suspension after the reaction and (2)

* Corresponding author. Tel.: +82 31 645 1432; fax: +82 31 645 1488.
E-mail address: jino.kim@kicet.re.kr (J.-H. Kim).

0272-8842/$36.00
doi:10.1016/j.ceramint.2012.01.042

particulate suspensions are not easily applicable to continuous processes. Thus, a photocatalyst in film form may be an excellent alternative for resolving these technical problems. The methods available for the fabrication of photocatalytic films include sol–gel [14], sputtering [15], e-beam evaporation [16], and aerosol deposition [17,18]. Among these, the aerosol deposition (AD) method is an effective technique that enables the fabrication of thin or thick film at room temperature with a high deposition rate and a strong adhesion to the substrate. The aerosol deposition method is based on the impact adhesion of sub- or micron particles accelerated by gas up to a subsonic velocity to a substrate. In addition, operation at room temperature makes it possible to fabricate a film without any phase change.

In this paper, $SrBi_2Nb_2O_9$ compounds synthesized by a solid-state reaction were used as a source material for aerosol and characterized by XRD and SEM analysis. $SiBi_2Ni_2O_9$ thin films were successfully fabricated from micron-sized powder at room temperature by aerosol deposition, and their photocatalytic activity was extensively investigated. The photocatalytic performances of the aerosol-deposited film were evaluated by measuring the photo-degradation of a Rhodamine B (Rh-B) aqueous solution with a UV–vis spectrophotometer.

2. Experimental

The polycrystalline samples of the photocatalysts were synthesized by a conventional solid state method from the starting materials of carbonates ($SrCO_3$, 99%) and oxides (Bi_2O_3, Nb_2O_5, 99.9%). A mixture of these starting materials in an appropriate molar ratio was finely ground in an agate mortar and pressed into pellets. The pellets were calcined at 900 °C for 15 h, 1000 °C for 15 h, and 1200 °C for 24 h, with intermittent grinding using an attrition mill for 2 h. Fig. 1(a) shows the X-ray diffraction pattern from $2\theta = 10^\circ$ to 80° of the prepared $SrBi_2Nb_2O_9$ compound. The XRD pattern of $SrBi_2Nb_2O_9$ was indexed with orthorhombic ($A2_1am$) SBN according to JCPDS card No. 89-8154 and no second phases such as Bi_2O_3, Nb_2O_5, and other possible Sr–B–Nb–O compounds were detected from the simulated pattern program of JADE 7 software. From the SEM analysis the particle size of $SrBi_2Nb_2O_9$ was found to be the range from 600 nm to 1 μm.

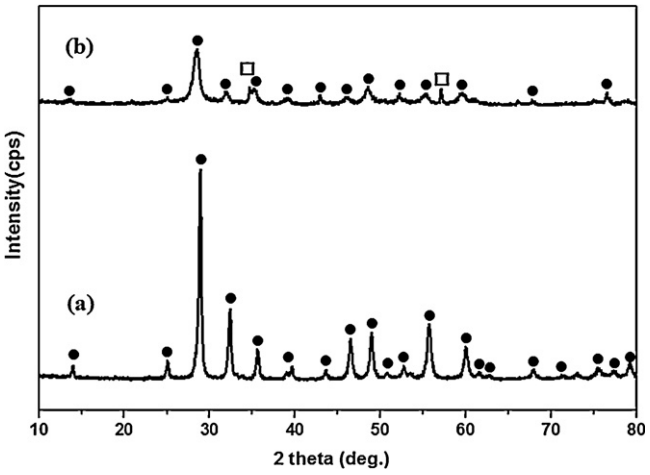

Fig. 1. X-ray diffraction patterns of the $SrBi_2Nb_2O_9$ samples (a) powders and (b) aerosol-deposited film (●, $SrBi_2(Nb_2O_9)$; □:, Al_2O_3).

The aerosol deposition (AD) apparatus employed in this study consists of three parts: an aerosol generator, a mass-flow controller, and a deposition chamber [19]. Aerosol is formed in the aerosol generator with a carrier gas and then transported into the deposition chamber. The chamber is then evacuated by a rotary pump with a mechanical buster, causing the aerosol to accelerate through a nozzle to collide with a substrate. Alumina (Al_2O_3) plates with dimension of 2 mm (t) × 10 mm (w) × 10 mm (h) were used as substrate. The carrier gas used in the deposition process was He and the consumption rate was 4–5 L/min. The working pressure and size of nozzle orifice were less 10 Torr and 20 mm × 0.4 mm, respectively. Phase analysis on aerosol-deposited $SrBi_2Nb_2O_9$ films was performed by X-ray diffractometer (Rigaku D/Max 2500) with Cu Kα radiation from $2\theta = 5^\circ$ to 80° at the step size of 0.016° and count time of 0.508 s. The morphology and absorption edge of the $SrBi_2Nb_2O_9$ samples were observed using a field emission scanning electron microscopy (FESEM, JEOL JSM 6701F) and a UV–vis spectrophotometer (Varian Cray 100 Conc.), respectively. The surface roughness (R_a) of the film was measured using a surface roughness profiler (KOSAKA Surfcorder ET 3000) three times for each sample with a scanning distance of 4 mm at different positions.

The photocatalytic performance tests were carried out by employing powders or film of $SrBi_2Nb_2O_9$ in 100 mL of 4×10^{-5} M Rhodamine B (Rh-B) solution. The Rh-B (purity, 99%) was purchased from Aldrich Co. and used as received (molecular formula: $C_{24}H_{31}ClN_2O_3$, molecular weight: 479.02 g/mol). The suspension was first stirred at 150 rpm in the dark for 30 min to ensure the saturated adsorption of Rh-B prior to illumination. Before irradiation, a time period of 1 h was allowed to ensure the establishment of adsorption–desorption equilibrium between the catalysts and Rh-B. A fluorescence lamp (LS-2000) with the intensity of less than 1 mW/cm^2 was used as the light source and a long-pass glass filter with 420 nm cut-off was employed to evaluate the photocatalytic activity in visible light range. The UV light source was a high pressure Hg lamp (125 W) that was placed 2 cm above the solution level. UV intensity at the film surface was ∼8 mW/cm^2. In order to guarantee maximum use of the radiation and to prevent the effects of external radiation, Al foil was used to cover the top of the reactor, which was open to air, as well as the sides and the bottom. Rh-B concentration with the irradiation time was measured by a UV–vis spectrophotometer.

3. Results and discussion

The XRD analysis on the powders and aerosol-deposited films of the $SrBi_2Nb_2O_9$ compound are shown in Fig. 1(a) and (b). The peak of the $SrBi_2Nb_2O_9$ powder was sharp and narrow, indicating a phase with a large crystallite size. Meanwhile, the as-deposited $SrBi_2Nb_2O_9$ film on Al_2O_3 plate showed small and broad peaks in comparison with the raw powders, despite being

deposited at room temperature. According to the Scherrer relation, these broad peaks imply that the film consisted of very small crystallite [20]. In the aerosol deposition (AD) method, ceramic particles are accelerated up to a velocity of few hundred m/s in a vacuum chamber and then collide with the substrate to make a film. The deposition mechanism of the AD is regarded as an impact consolidation through the fracture and plastic deformation of primary particles [21]. It is well known that the high impact energy of the particle collision occurring during deposition results in the small grain size of the films. Toyoda et al. reported that the increase in FWHM, i.e., decrease in apparent crystallite size, results in enhancement in photoactivity, probably because of high surface area, which can contact with Rh-B molecules, and high possibility of recombination of excited electrons and holes by the scattering at structural defects [22]. Ryu et al. reported the presence of peak broadness from XRD pattern of the aerosol-deposited TiO_2 film, which is in good agreement with the TEM (transmission electron microscopy) and SAED (selected area electron diffraction) measurements showing the coexistence of nanocrystalline and amorphous phase [17,18]. In addition, the formation of a new phase in the as-deposited SrBi2Nb2O9 film was not observed as shown in Fig. 1(b), indicating that the AD method is a novel process which might replace high temperature process.

Fig. 2 shows micrographs of the aerosol-deposited $SrBi_2Nb_2O_9$ film on Al_2O_3 support. Ryu et al. reported a well developed network microstructure in the aerosol-deposited TiO_2 film, along with the absence of any micro-cracks or pores [18]. Fig. 2(a) shows that the AD method produced a porous $SrBi_2Nb_2O_9$ film with micro-cracks or pores. A network microstructure was observed. The high-resolution SEM image of the aerosol-deposited $SrBi_2Nb_2O_9$ film in Fig. 2(b) shows that the submicron particles were uniformly deposited on the Al_2O_3 support, indicating that the fragmentation of the $SrBi_2Nb_2O_9$ powders occurred during the AD method. The average surface roughness (R_a) of the aerosol-deposited $SrBi_2Nb_2O_9$ film was 3420 Å which was almost 1–2 orders of magnitude higher than that of typical sputtered (R_a of several tens nm) or sol–gel derived (R_a several nm) films [23,24]. In general, it is expected that an increase in surface roughness leads to a greater surface area. As shown in Fig. 2(c), the cross-sectional micrographs of the aerosol-deposited $SrBi_2Nb_2O_9$ film exhibit fairly uniform thickness of approximately 5 μm.

The optical absorption property of the material and the migration of the light-induced electrons and holes are considered to be the most important factor for controlling a photocatalytic reaction. These are related to the electronic characteristics of the material [25,26]. Fig. 3 shows the diffuse reflectance spectra of both the as-synthesized powder and the aerosol-deposited film of $SrBi_2Nb_2O_9$. The maximum wavelength required to promote an electron depends upon the band-gap energy E_{bg} of the photocatalyst and is given by:

$$E_{bg}[\mathrm{eV}] = \frac{hv}{\lambda}$$

where λ is the wavelength in nanometer.

We can use the following formula to calculate the band gap energy of both the as-synthesized powder and the aerosol-deposited film of $SrBi_2Nb_2O_9$.

$$\alpha hv = A(hv - E_{bg})^{1/2}$$

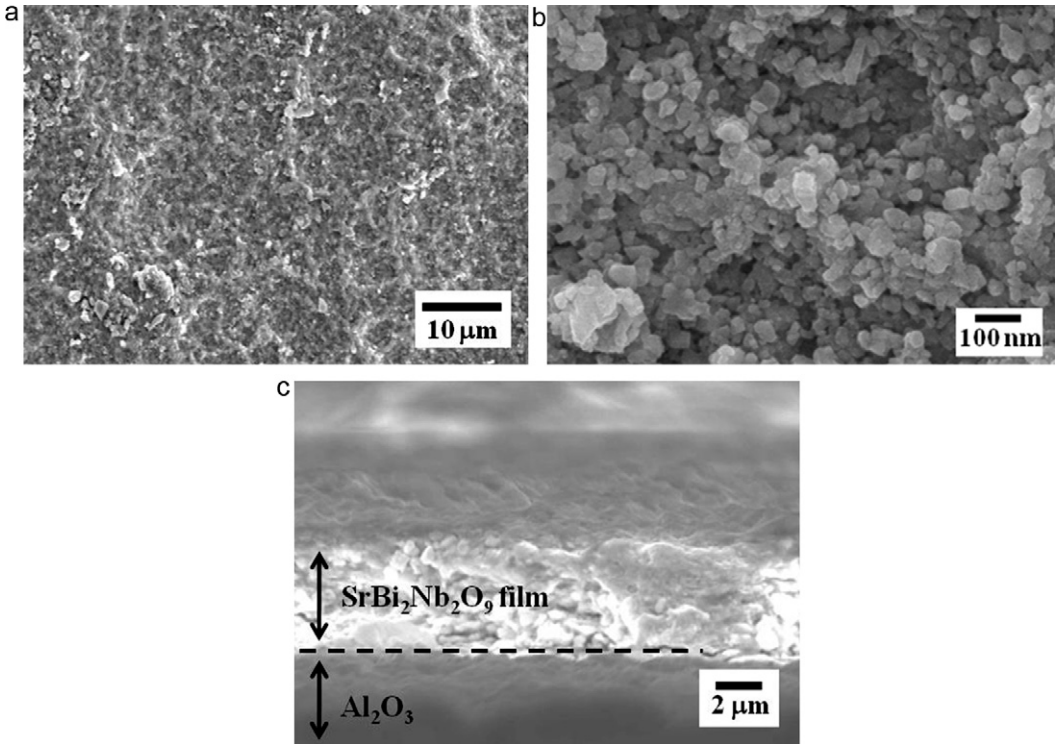

Fig. 2. FESEM images of aerosol-deposited the $SrBi_2Nb_2O_9$ film: (a) surface (low magnitude), (b) surface (high magnitude) and (c) cross-section.

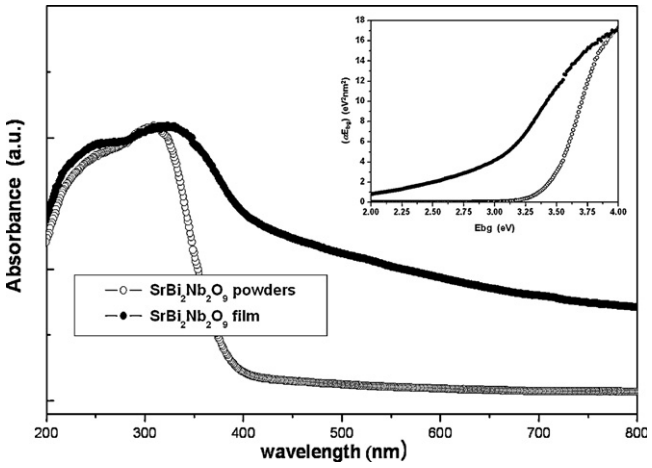

Fig. 3. UV–vis diffuse reflectance spectra and band-gap energy of the $SrBi_2Nb_2O_9$ powder and aerosol-deposited film.

where α, h, ν, E_{bg}, and A are the absorption coefficient, Plank's coefficient, light frequency, band gap energy, and a constant, respectively [34].

Therefore, the band gap energy (E_{bg}) can be calculated from a plot $(\alpha h\nu)^2$ versus E_{bg} for direct band gap transition, as shown in figure inset in Fig. 3. For $ABi_2Nb_2O_9$ (A = Sr, Ba), the calculated band structure indicates a direct-gap semiconductor materials [12]. The value of E_{bg} extrapolated to $\alpha = 0$ gives an absorption energy, which indicates to a band gap energy. The band gap energy of $SrBi_2Nb_2O_9$ powder is 3.4 eV, which is fairly close to literature value [12]. As shown in Fig. 3, compared to the $SrBi_2Nb_2O_9$ powders, an additional visible light absorption tail appears in the aerosol-deposited $SrBi_2Nb_2O_9$ film with a slight red-shift in the pristine absorption edge. The band gap energy of aerosol-deposited $SrBi_2Nb_2O_9$ film is estimated 2.35 eV, which indicates the better photocatalytic property than the aerosol-deposited TiO_2 film [18]. Compared with the aerosol-deposited $SrBi_2Nb_2O_9$ powder, it can be expected that the aerosol-deposited $SrBi_2Nb_2O_9$ film should have enhanced photocatalytic potential in both UV and visible light. The additional visible light absorption tail of the photocatalysts indicates that, in this case, only some localized states in the band gap are responsible for the visible light absorption [18,27,28]. Bickley et al. reported that the presence of amorphous phase in a complex microstructure attributes to the formation of localized Anderson state, which may increase the life-time of photo-excited electron–hole pairs and thereby enhance the photocatalytic activity. In addition, Ryu et al. reported that the aerosol-deposited TiO_2 film showed the coexistence of nanocrystallites and amorphous, and both the absorbance edge and tail behavior were shifted towards the visible region. In conclusion, the enhanced photocatalytic performance of the aerosol-deposited $SrBi_2Nb_2O_9$ film was attributed not only to the exceptionally rough and porous microstructure, but also to the presence of the nanocrystalline and amorphous region.

Photocatalytic activities were evaluated by monitoring the degradation of a model dye Rh-B upon irradiation with UV and visible light (>420 nm) following a procedure reported in the literature [29,30]. The solutions with photocatalysts were kept in the dark for 30 min before irradiation. No change in the concentration of the solution was observed in the absence of a photocatalyst or in the dark experiment, indicating that the decomposition of Rh-B only proceeds via the photo-excited semiconductor catalyst. As shown in Fig. 4(a) and (b), the peak height gradually is decreased with the irradiation time, suggesting the degradation of Rh-B by the photocatalytic activity of the aerosol-deposited $SrBi_2Nb_2O_9$ film. Under UV illumination, Rh-B was decomposed much more quickly compared to the irradiation under visible light. The spectrum curves were almost flattened after 2 h, as shown in Fig. 4(a). Fig. 4 also shows that the peak position shifted toward lower wavelengths with increased irradiation time, indicating the formation of photo-degradation intermediate species with absorption peaks between 502 nm and 541 nm [31,32].

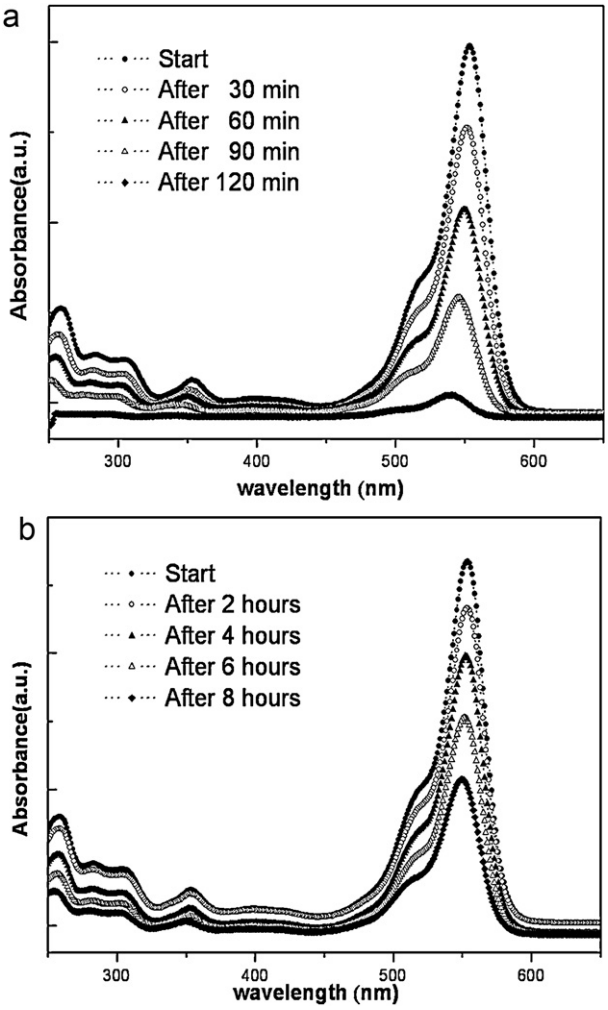

Fig. 4. UV–vis diffuse spectral change of Rh-B during the photocatalytic reduction process catalyzed by the $SrBi_2Nb_2O_9$ film as function of illumination time: (a) UV-light irradiation and (b) visible-light irradiation.

Fig. 5 represents the decrease of Rh-B (C/C_0) as a function of irradiation time over the aerosol-deposited $SrBi_2Nb_2O_9$ film. Here, C is the absorption of Rh-B at the wavelength of 553 nm and C_0 is the absorption of Rh-B after the adsorption equilibrium on the aerosol-deposited $SrBi_2Nb_2O_9$ film before

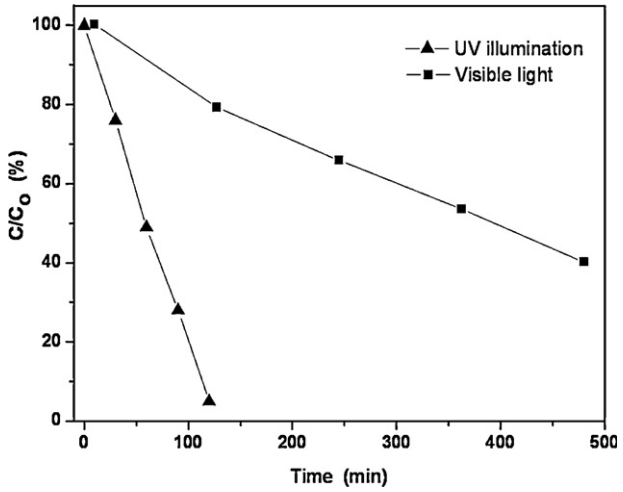

Fig. 5. Variation in the concentration of Rh-B catalyzed by the aerosol-deposited $SrBi_2Nb_2O_9$ film under different conditions (UV- and visible-light irradiation).

irradiation. As evident in Fig. 5, under UV illumination, Rh-B was almost completely degraded after 2 h of irradiation on the aerosol-deposited $SrBi_2Nb_2O_9$ film. Also, the photo-induced degradation of Rh-B was significantly slower with the irradiation of UV light as compared to visible light. After 480 min, only about 42% of Rh-B was degraded over the aerosol-deposited $SrBi_2Nb_2O_9$ film. However, the photocatalytic activity of the aerosol-deposited $SrBi_2Nb_2O_9$ film is superior to that of the $SrBi_2Nb_2O_9$ powders. Hu et al. reported that two procedures are involved in the degradation of Rh-B: the de-ethylation and the cleavage of the conjugated chromophore structure [33]. Usually these two procedures take place simultaneously in the presence of a photocatalyst under irradiation, and this cooperative effect results in the decrease of absorbance at the wavelength of 553 nm with the prolonged irradiation time. Ryu et al. reported the observation of an exceptionally rough network microstructure and nano-projections that were able to support enhanced loading of organic contaminants onto the surface of aerosol-deposited TiO_2 film. Therefore, the enhancement of photocatalytic destruction of Rh-B with the $SrBi_2Nb_2O_9$ film is ascribed to the existence of nano-grained film resulting from the aerosol deposition method.

4. Conclusion

The $SrBi_2Nb_2O_9$ compound with perovskite-type layered structure was synthesized by solid state reaction, and network microstructure film was fabricated by aerosol deposition method. The FESEM image of the aerosol-deposited $SrBi_2Nb_2O_9$ film shows that the submicron particles were uniformly deposited on the Al_2O_3 support, indicating that the fragmentation of $SrBi_2Nb_2O_9$ powders occurred during the AD method. The average surface roughness (R_a) of the aerosol-deposited $SrBi_2Nb_2O_9$ film was 3420 Å which was almost 1–2 orders of magnitude higher than that of typical sputtered (R_a of several tens nm) or sol–gel derived (R_a several nm) films, indicating an increase in surface roughness. This leads to a higher surface area. The main adsorption edges of the diffuse reflectance spectra of the powder and the aerosol-deposited film with $SrBi_2Nb_2O_9$ were approximately 365 nm (~3.4 eV) and 530 nm (~2.35 eV), respectively. Compared to the $SrBi_2Nb_2O_9$ powders, an additional visible light absorption tail appears in the aerosol-deposited $SrBi_2Nb_2O_9$ film with a slight red-shift in the pristine absorption edge. The band gap adsorption edge of the aerosol-deposited $SrBi_2Nb_2O_9$ film is estimated to be ~530 nm corresponding to a band gap energy of ~2.35 eV. It can be expected that the aerosol-deposited $SrBi_2Nb_2O_9$ film should have enhanced photocatalytic potential in both UV and visible light. The enhanced photocatalytic degradation of aerosol-deposited film was attributed to the small grain size and the network microstructure which is capable of supporting the enhanced loading of organic contaminants on the aerosol-deposited film. This type of immobilized photocatalyst has achieved valuable experimental results in treating Rh-B dyed waste water, implying prospects for water purification applications.

Acknowledgement

This subject is supported by Korea Ministry of Environment as ‘‘The Eco-Innovation project (Global Top project), GT-SWS-11-01-004-0’’.

References

[1] K. Handa, A. Fujishima, Electrochemical photolysis of water at a semiconductor, Nature 238 (1972) 37–38.
[2] M.R. Hoffmann, S.T. Martin, W. Choi, D.W. Bahnemann, Environmental Applications of Semiconductor Photocatalysis, Chem. Rev. 95 (1995) 69–96.
[3] Z. Zou, J. Ye, K. Sayama, H. Arakawa, Direct splitting of water under visible light irradiation with an oxide semiconductor photocatalyst, Nature 414 (2001) 625–627.
[4] S.F. Chen, W. Zhao, S.J. Zhang, W. Liu, Preparation, characterization and photocatalytic activity of N-containing ZnO powder, Chem. Eng. J. 148 (2009) 263–269.
[5] M.M. Viana, V.F. Soares, N.D.S. Mohallem, Synthesis and characterization of TiO_2 nanoparticles, Ceram. Int. 36 (2010) 2047–2053.
[6] T. Yazawa, F. Machida, N. Kubo, T. Jin, Photocatalytic activity of transparent porous glass supported TiO_2, Ceram. Int. 35 (2009) 3321–3325.
[7] Y. Liu, J. Ma, Z. Liu, C. Dai, Z. Song, Y. Sun, J. Fang, J. Zhao, Low-temperature synthesis of $BiVO_4$ crystallites in molten salt medium and their UV–vis absorption, Ceram. Int. 36 (2010) 2073–2077.
[8] K.G. Kanade, J.O. Baeg, K.J. Kong, B.B. Kale, S.M. Lee, S.J. Moon, C.W. Lee, S.H. Yoon, A new layer perovskites $Pb_2Ga_2Nb_2O_{10}$ and $RbPb_2Nb_2O_7$: an efficient visible light driven photocatalysts to hydrogen generation, Int. J. Hydrogen Energy 33 (2008) 6904–6912.
[9] K. Gurunathan, J.O. Baeg, S.M. Lee, E. Subramanian, S.J. Moon, K.J. Kong, Visible light active pristine and Fe^{3+} doped $CuGa_2O_4$ spinel photocatalysts for solar hydrogen production, Int. J. Hydrogen Energy 33 (2008) 2646–2652.
[10] A. Ishikawa, T. Takata, J.N. Kondo, M. Hara, H. Kobayashi, K. Domen, Oxysulfide $Sm_2Ti_2S_2O_5$ as a stable photocatalyst for water oxidation and reduction under visible light irradiation, J. Am. Chem. Soc. 124 (2002) 13547–13553.
[11] B. Aurivillius, Mixed bismuth oxides with lauer lattices, Ark. Kemi. 1 (1949) 463–471.

[12] Y. Li, G. Chen, H. Zhang, Z. Lu, Band structure and photocatalytic activities for H_2 production of $ABi_2Nb_2O_9$ (A = Ca, Sr Ba), Int. J. Hydrogen Energy 35 (2010) 2652–2656.
[13] W. Wu, S. Liang, X. Wang, J. Bi, P. Liu, L. Wu, Synthesis, structures and photocatalytic activities of microcrystalline $ABi_2Nb_2O_9$ (A = Sr Ba) powders, J. Solid State Chem. 184 (2011) 81–88.
[14] C. Millon, D. Riassetto, G. Berthome, F. Roussel, M. Langlet, The photocatalytic activity of sol–gel derived photo-platinized TiO_2 films, J. Photochem. Photobiol. A 189 (2007) 334–338.
[15] F. Meng, F. Lu, Characterization and photocatalytic activity of TiO_2 thin films prepared by RF magnetron sputtering, Vacuum 85 (2010) 84–88.
[16] M.W. Pyun, E.J. Kim, D.H. Yoo, S.H. Hahn, Oblique angle deposition of TiO_2 thin films prepared by electron-beam evaporation, Appl. Surf. Sci. 257 (2010) 114–1153.
[17] J.H. Ryu, K.Y. Kim, B.D. Hahn, J.J. Choi, W.H. Yoon, B.K. Lee, D.S. Park, C. Park, Photocatalytic nanocomposite thin films of TiO_2-β-calcium phosphate by aerosol-deposition, Catal. Commun. 10 (2009) 596–599.
[18] J.H. Ryu, D.S. Park, B.D. Hahn, J.J. Choi, W.H. Yoon, K.Y. Kim, H.S. Yun, Photocatalytic TiO_2 thin films by aerosol-deposition: from micron-sized particles to nano-grained thin film at room temperatures, Appl. Catal. B 83 (2008) 1–7.
[19] J.H. Kim, Y.M. Kang, B.G. Kim, S.H. Lee, K.T. Hwang, Preparation of dense composite membrane with Ba-cerate conducting oxide and rapidly solidified Zr-based alloy, Int. J. Hydrogen Energy 36 (2011) 10129–10135.
[20] J.J. Choi, B.D. Hahn, W.H. Yoon, B.K. Lee, D.S. Park, Preparation and characterization of piezoelectric ceramic-polymer composite thick films by aerosol deposition for sensor application, Sens. Actuators A 153 (2009) 89–95.
[21] K. Mihara, T. Hoshina, H. Takeda, T. Tsurumi, Controlling factors of film-thickness in improved aerosol deposition method, J. Ceram. Soc. Jpn. 117 (2009) 868–872.
[22] M. Toyoda, Y. Nanbu, Y. Nakazawa, M. Hirono, M. Inagaki, Effect of crystallinity of anatase on photoactivity for methyleneblue decomposition in water, Appl. Catal. B 49 (2004) 227–232.
[23] Y. Hoshi, T. Kiyomura, ITO thin films deposited at low temperatures using a kinetic energy controlled sputter-deposition technique, Thin Solid Films 411 (2002) 36–41.
[24] J.X. Liu, D.Z. Yang, J. Feng, Sol–gel deposited TiO_2 film on NiTi surgical alloy for biocompatibility improvement, Thin Solid Films 429 (2003) 225–230.
[25] J.W. Tang, Z.G. Zou, J.H. Ye, Efficient photocatalytic decomposition of organic contaminants over $CaBi_2O_4$ under visible-light irradiation, Angew. Chem. Int. Ed. 43 (2004) 4463–4466.
[26] N. Ma, X. Fan, X. Quan, Y. Zhang, Ag–TiO_2/HAP/Al_2O_3 bioceramic composite membrane: fabrication characterization and bactericidal activity, J. Membr. Sci. 336 (2009) 109–117.
[27] H. Irie, Y. Watanabe, K. Hashimoto, Nitrogen-concentration dependence on photocatalytic activity of $TiO_{2-x}N_x$ powders, J. Phys. Chem. B 107 (2003) 5483.
[28] R.I. Bickley, T. Gonzalez-Carreno, J.S. Lee, L. Palmisano, R.J.D. Tilley, A structural investigation of titanium dioxide photocatalysts, J. Solid State Chem. 92 (1991) 178–190.
[29] C. Xu, D. Zou, L. Wang, H. Luo, T. Ying, γ-Bi_2MoO_6 nanoplates: surfactant-assisted hydrothermal synthesis and optical properties, Ceram. Int. 35 (2009) 2099–2102.
[30] J.S. Wu, C.H. Liu, K.H. Chu, S.Y. Suen, Removal of cationic dye methyl violet 2B from water cation exchange membranes, J. Membr. Sci. 309 (2008) 239–245.
[31] T. Tsuzuki, Z. Smith, A. Parker, R. He, X. Wang, Photocatalytic activity of manganese-doped ZnO nanocrystalline powders, J. Aust. Ceram. Soc. 45 (2009) 58–62.
[32] F. Chen, J. Zhao, H. Hidaka, Highly selective deethylation of rhodamine B: adsorption and photooxidation pathways of the dye on the TiO_2/SiO_2 composite photocatalyst, Int. J. Photoenergy 5 (2003) 209–217.
[33] X.F. Hu, T. Mohamood, W.H. Ma, C.C. Chen, J.C. Zhao, Oxidative decompositions of rhodamine B dye in the presence of VO_2^+ and/or Pt(IV) under visible light irradiation: N-deethylation chromophore cleavage, and mineralization, J. Phys. Chem. B 110 (2006) 26012–26018.
[34] M.L. Chen, W.C. Oh, Synthesis and highly visible-induced photocatalytic activity of CNT–CdSe composite for methylene blue solution, Nanoscale Res. Lett. 6 (2011) 1–8.